

Self-Consistent Field Analysis of Ionic Surfactant Adsorption Regulation in the Aqueous Film between Two Neutral Solids

William J. Lokar,^{*,†,‡} Luuk K. Koopal,[†] Frans A. M. Leermakers,[†] and William A. Ducker[‡]

Laboratory of Physical Chemistry and Colloid Science, Wageningen University, Dreijenplein 6, 6703 HB Wageningen, The Netherlands, and Department of Chemistry, Virginia Tech, Blacksburg, Virginia 24061

Received: November 7, 2003; In Final Form: January 12, 2004

Self-consistent field theory for adsorption and association is utilized to calculate the adsorption of the ionic surfactant ($C_{16}P_3^+$) on two neutral, slightly hydrophobic solids separated by a thin aqueous film and immersed in an infinite reservoir of aqueous 1:1 electrolyte. The change in surfactant adsorption as a function of the separation between the solids is discussed in relation to the forces between the solids as well as the shape of the adsorption vs concentration curve for an isolated surface. Surfactants desorb from the surface as the electrostatic potential in the gap between the surfaces is increased due to the overlap of electric potential profiles. Changes in adsorption are most sensitive to solid–solid separation when the surfactant concentration is near the step in the adsorption isotherm. Adsorbed surfactant layers also become thinner as the surfaces approach, and the adsorbed amount can change in more complex ways when the adsorbed layers come into contact.

Introduction

Colloidal suspensions are important in many industries. Latex paints, milk, ceramics, and clays are all examples of colloidal materials. The stability of colloidal suspensions is dictated by the forces that exist between the particles. These forces can vary from simple Derjaguin, Landau, Verwey, and Overbeek theory (DLVO) forces (electric double-layer and van der Waals forces) to more complicated forces such as hydration, hydrophobic, and depletion forces. In order for the stability of colloidal suspensions to be controlled, the forces must be able to be manipulated. This is commonly done by means of surfactant or polymer adsorption onto the particles from aqueous solution.

Surfactants and polymers can change the interaction forces in several ways. Adsorption of ionic species can modify the electric double-layer potential, polymers can stabilize suspensions by steric means, and adsorption can modify the van der Waals interactions. If adsorption or desorption changes the characteristics of the particles in a way that results in a lower (more negative) interaction energy, we say that the forces have been regulated. The most widely known case of regulation is the regulation of charge on colloidal particles by ions in solution.¹ Regulation of surfactant adsorption has been discussed in the literature by applying a thermodynamic relation originally derived by Hall² and Ash et al.³ These studies focused on cetyltrimethylammonium bromide ($C_{16}TAB$) adsorption on mica⁴ and silica.^{5–8} The most extensive studies to date have been conducted by Ducker and co-workers.^{9–11} These studies have been specifically targeted to elucidate the effects of ionic strength, chain length, and pH on surfactant adsorption regulation.

Until now, adsorption of surfactants as a function of solid–solid separation (proximal adsorption) has not been studied thoroughly from a theoretical standpoint. For systems involving chain molecules such as surfactants and polymers, “exact” theories become extremely complicated and very expensive in terms of computer power and time.

There exists a relatively inexpensive theory by Scheutjens and Fleer^{12,13} that has been designed originally for studies of polymer adsorption to solid surfaces and self-association of surfactants. Studies have been routinely conducted using the Scheutjens–Fleer (SF) method to model lipid bilayer membranes,^{14–16} self-assembly of surfactants in solution and at interfaces,^{17–22} polyelectrolyte adsorption,^{23,24} polymer brushes,^{25,26} wettability,²⁷ colloidal stability,²⁸ and liquid chromatography.²⁹

In this paper, we will use the SF approach to look at how the interaction of two identical, neutral surfaces is regulated by the adsorption of ionic surfactants.

The self-consistent field theory for adsorption and association (SCFA) is based on lattice and mean-field approximations. The particular lattice geometry selected dictates the geometry of any aggregates formed (whether on surfaces or in the bulk). Here we look at a system of two flat homogeneous surfaces some separation, H , apart. Density fluctuations are ignored parallel to the surface (mean-field) and permitted perpendicular to it (z direction). In these calculations, gradients in the densities and self-consistent potentials are permitted in the z direction only. While this one-dimensional gradient does have serious limitations in describing adsorption of single surfactants, the approximation is reasonable for monolayer or bilayer coverages.

In SCFA theory, all molecular species are represented as a segment or sequence of connected segments. These segments are arranged on a lattice to enable conformational probabilities to be calculated. All lattice sites are filled with a segment of a molecule, ion, or solvent. Therefore, the volume fractions of all segments will always sum to unity (incompressibility approximation).

There are two basic lattice parameters that affect the calculations. One is the lattice site size, and the other is the step probabilities between adjacent sites. In the case of the flat lattice, the fraction of contacts that one site has with sites in a previous or following layer (λ_{-1} and λ_1) is naturally independent of z ; however, for the spherical and cylindrical cases, the fraction of contacts is a function of z . Details are given elsewhere.³⁰ The fraction of contacts in an adjacent layer (λ_1), and within the same layer (λ_0), is governed by the type of lattice chosen for

* Author to whom correspondence may be addressed. E-mail: wlokar@vt.edu.

[†] Wageningen University.

[‡] Virginia Tech.

the calculations. For this particular study we have chosen a face-centered cubic lattice in which $\lambda_{-1} = \lambda_0 = \lambda_1 = 1/3$. We have chosen a lattice with a cross section of 0.31 nm so that, when the lattice is fully occupied by water, we obtain a concentration of 55.5 M as found experimentally.

We will now briefly discuss some physical details of the calculations. We define a dimensionless density, $\phi_A(z)$, as the volume fraction of segments of type A (not molecules) in layer z . For bulk volume fractions, $\phi_A(z)$ is no longer a function of z and now the notation becomes ϕ_A^b . To account for the differences between each layer, z , and the bulk, we define the mean potential energy (Gibbs energy per segment) difference required to move a segment A from the bulk to layer z as $u_A(z)$

$$u_A(z) = u'(z) + kT \sum_B (\langle \phi_B(z) \rangle - \phi_B^b) \chi_{AB} + v_A e \psi(z) - \frac{1}{2} (\epsilon_A - \epsilon_0) E(z)^2 \quad (1)$$

The first term represents the volume work needed to insert a segment at position z . It is independent of the segment type (all segments have the same size). It is adjusted only to enforce that the volume fractions sum to unity at each z . The second term accounts for contact interactions between segments in adjacent layers. The magnitude of the interaction between segments of types A and B is governed by the Flory–Huggins interaction parameter χ_{AB} .³¹ By realization that a segment of type A at layer z can interact with segments of type B in layers $z' = z-1, z, z+1$, we should average over three layers. Such an average is represented by the angular brackets

$$\langle \phi(z) \rangle = \lambda_{-1} \phi(z-1) + \lambda_0 \phi(z) + \lambda_1 \phi(z+1) \quad (2)$$

The first two terms in eq 1 comprise the nonelectrostatic portion of the potential and are discussed in greater detail elsewhere.³² The third term represents the classical electrostatic work needed to bring an ionic species to layer z . $\psi(z)$ is the electrostatic potential, e is the elementary charge, and v_A is the valence of segment A. The fourth term expresses the free-energy gain due to polarization when a segment is transferred from the bulk to a position z . Because of the electric field, $E(z) = -(\partial\psi(z)/\partial z)$, the segments polarize. This occurs spontaneously (hence the negative sign). The polarization is proportional to the difference between the permittivity of A and that of a vacuum, $(\epsilon_A - \epsilon_0)$, and the field strength, $E(z)$. The energy gain is again proportional to $E(z)$. Therefore, the polarization term is given by $(\epsilon_A - \epsilon_0)E(z)^2$. On the other hand, the entropic cost of orienting a dipole is $1/2$ this value, hence the presence of the $1/2$ in the fourth term.

The third and fourth terms in eq 1 are rather straightforward; however, $\psi(z)$ and $E(z)$ must be determined within each layer. These quantities follow from solving the discrete version of the Poisson equation

$$-\sigma(z) = \frac{\partial \epsilon(z) \partial \psi(z)}{\partial z^2} \quad (3)$$

One way to look at it is that the electrostatic potentials are calculated from a model considering multiple Stern layers. According to eq 3, the net charge and the capacitance of each layer are required. The local charge density is calculated from the local volume fractions per segment type

$$\sigma(z) = \sum_A v_A e \phi_A(z) \quad (4)$$

The charge is considered to lie at the midpoint of each layer, and the permittivity of each layer is given by a volume fraction

weighted average of the permittivity of each species

$$\epsilon(z) = \sum_A \epsilon_A \phi_A(z) \quad (5)$$

The details of evaluating $\psi(z)$ are given elsewhere.³⁰

When dealing with chain molecules, it is important to account for the chain conformations in a reasonable manner. Basically, one should consider the statistical weight of each possible conformation of each molecule. The naïve way to do this is to generate each conformation separately and add up the potential energies felt by each of its segments. The overall potential energy is used in the Boltzmann equation to find the statistical weight for each specified conformation. The statistical weights are subsequently found by normalizing all the Boltzmann weighted potential energies. This procedure is extremely time consuming. The alternative is to use a Markov approximation. The conformations of the surfactant molecules are then accounted for by means of a step-weighted random walk.¹² In other words, this procedure generates all possible conformations and attaches the proper statistical weights to them in a scheme, which takes only order N operations, where N is the number of segments in the chain. It is instructive to outline this formalism that sometimes is referred to as the propagator method.

We start by introducing the segment-type dependent-weighting factor, $G_A(z)$, as a Boltzmann expression in which the segment potential given by eq 1 is used

$$G_A(z) = \exp \left[\frac{-u_A(z)}{kT} \right] \quad (6)$$

This quantity needs to be generalized to a ranking number and molecule type dependent quantity $G_i(z,s)$, where the molecules will be denoted by the index i and the segments in the chain will obtain the ranking numbers $s = 1, \dots, N_i$ (the number of segments in molecule i). By introduction of the chain architecture operator $\delta_{s,i}^A$, which takes the value unity when segment s of molecule i is of type A and is zero otherwise, we can identify

$$G_i(z,s) = \sum_A \delta_{s,i}^A G_A(z) \quad (7)$$

Next, there are two complementary chain end distribution functions $G_i(z,s|1)$ and $G_i(z,s|N)$ that contain the overall statistical weights of all possible conformations of fragments $s' = 1, \dots, s$ and $s' = N, \dots, s$ respectively, with the requirement that segment s of molecule i is at position z . These end-point distribution functions are generated by two propagators

$$\begin{aligned} G_i(z,s|1) &= G_i(z,s) \langle G_i(z,s-1|1) \rangle \\ G_i(z,s|N) &= G_i(z,s) \langle G_i(z,s+1|N) \rangle \end{aligned} \quad (8)$$

where the angular brackets have the same meaning of a three-layer average as in eq 1 but now operate on the end-point distributions.

These propagators are initiated by using the free segment distribution function for the first and last segment respectively

$$\begin{aligned} G_i(z,1|1) &= G_i(z,1) \\ G_i(z,N|N) &= G_i(z,N) \end{aligned} \quad (9)$$

The volume fraction of segment s of molecule i in layer z follows from the composition of two complementary end point distribution functions

$$\phi_i(z,s) = C_i \frac{G_i(z,s|1)G_i(z,s|N)}{G_i(z,s)} \quad (10)$$

Here the denominator corrects for the fact that both end point distribution functions used in eq 10 have accounted for the potential energy felt by segment s already whereas this weight should appear just once. The normalization constant C_i is determined from either information available on the number of molecules of type i (per unit area) in the system n_i or its density in the bulk

$$C_i = \frac{n_i}{\sum_z G_i(z,1|N)} = \frac{\phi_i^b}{N_i} \quad (11)$$

Here $\sum_z G_i(z,1|N)$ is the single chain partition function.

The volume fractions that depend on the segment type follow from the ones computed in eq 10

$$\phi_A(z) = \sum_i \sum_s \phi_i(z,s) \delta_{s,i}^A \quad (12)$$

The overall densities of a molecule of type i follow simply from summing over all its segments

$$\phi_i(z) = \sum_s \phi_i(z,s) \quad (13)$$

As is apparent from looking at eqs 1, 6, and 10, the volume fractions in each layer depend on the choice of the mean potential in each layer, which in turn depends on the volume fractions. Therefore, an iterative process is required, which obtains a self-consistent set of potentials and volume fractions that optimizes the partition function of the system. From the partition function, it is possible to extract all thermodynamic quantities of interest. Below we will be interested in the way surfactants influence the free energy of interaction of two identical surfaces. It is essential to mention that in computing this quantity we are going to fix all the chemical potentials in the system by maintaining equilibrium with an infinite reservoir. In this case, the free energy of interaction for a system with wall-to-wall separation, H , follows from the difference between the grand potential at separation H , $\gamma(H)$, and that at infinite separation, $\gamma(\infty)$

$$F_{\text{int}}(H) = \Delta\gamma(H) \quad (14)$$

$$\Delta\gamma(H) = \gamma(H) - \gamma(\infty) \quad (15)$$

Note here that the grand potentials for both surfaces are to be considered. The grand potential follows from a summation over the grand potential density

$$\gamma(H) = - \sum_{z=1}^H \Pi(z) \quad (16)$$

The grand potential density is a function of the segment densities and the segment potentials, including the electrostatic contributions and the short-range interactions. The grand potential density is given as

$$\begin{aligned} \Pi(z) = & kT \sum_i \frac{(\phi_i(z) - \phi_i^b)}{N_i} + \sum_A u_A(z) \phi_A(z) - \frac{1}{2} \sigma(z) \psi(z) - \\ & \frac{1}{2} kT \sum_A \sum_B \chi_{AB} [\phi_A(z) (\langle \phi_B(z) \rangle - \phi_B^b) - \phi_B^b (\phi_B(z) - \phi_B^b)] \quad (17) \end{aligned}$$

TABLE 1: χ Parameters for the 420 and 031 Surfaces

segment	C (420) (031)		P (420) (031)		S (420) (031)		W (420) (031)		K, B (420) and (031)
C			2	2	-2	-3	1.9	1.9	2
(tails)									
P (heads)	2	2			-4	0	0	0	0
S (surface)	-2	-3	-4	0			0	-1	0
W (water)	1.9	1.9	0	0	0	-1			0
K, B (salt ions)	2	2	0	0	0	0	0	0	

In this paper, we present values for the adsorption of a particular species. This value is calculated by summing the excess volume fraction of the segments, of a particular species, i , over all layers and dividing by the number of segments that comprise a single molecule, N_i , and the square of the lattice site cross section

$$\Gamma_i = \frac{\sum_z \phi_i(z) - \phi_i^b}{a_s^2 N_i} \quad (18)$$

Parameters

The results of the SCFA analysis depend strongly upon the choice of several molecule- and system-specific parameters. First, we will discuss our parameter choices for the surfactant, which are shown in Table 1. We model a cationic surfactant as a sequence of segments of two different types. One segment is given aliphatic characteristics (C) and the other more hydrophilic characteristics (P). Our surfactant is modeled as 16 C units attached to 3 P units, $C_{16}P_3$. The P units each have a charge equal to $+1/3$, bringing the total net charge to $+1$ for the surfactant. Such a headgroup has been used previously to model cationic surfactants with this theory.²⁰ In addition, the system is comprised of two other molecules that introduce 3 other segments: a solvent segment, W, and two segments, K and B, that represent salt ions. K possesses a valence of $+1$ and B a valence of -1 . Segments K and B are independent of each other (strong electrolyte). In addition, the permittivity must be chosen for each segment. The permittivity for the solvent and aliphatic segments is set to $80\epsilon_0$ and $2\epsilon_0$, respectively. The permittivity for segments K, B, and P is set to $40\epsilon_0$. Because of the dilute nature of these segments in the system, this choice has little effect on the bulk critical micelle concentration (cmc) over a range of 10 – $80\epsilon_0$. Therefore, we have chosen a value in the middle.

As stated earlier, the short-range contact interactions between segments are given by the Flory–Huggins χ parameters, χ_{AB} . The χ parameters for segments A' ($A' = K, B$, and P) with respect to the solvent segment W are all set to 0, $\chi_{WA'} = 0$. Therefore, no preferential interaction is given for these segments with water. Furthermore, the χ parameters for A' with respect to the aliphatic C segments are set to 2, $\chi_{CA'} = 2$. This means that there is a repulsion between the aliphatic chain segments and the hydrophilic salt and headgroup segments.

Perhaps the most crucial parameter selection for surfactants is the choice for χ_{CW} . The selection of such a parameter should ensure reasonable behavior of the surfactant with respect to experimental conditions, such as the effect of chain length or ionic strength on the cmc. We have determined that a value between 1.9 and 2 yields the most accurate behavior with respect to the chain-length dependence of the cmc. This value is slightly lower than the value of 2.3 suggested by Tanford.³³ In addition, the use of a value of 2 or higher results in lattice artifacts that

arise as the result of the sharpness of the aliphatic–water interface being the same order as the lattice size. Therefore, we have chosen a value of 1.9 for our calculations to avoid such complications.

In this paper, we will discuss the effects of solid–solid interactions upon the adsorption of the charged surfactant onto an uncharged surface. We will present two cases with slightly different surface parameters in order to illustrate the effect of some of the surface parameters.

(1) The first surface that we model has a somewhat hydrophobic character. The surface segments, S , are confined to the zeroth and $(H + 1)$ th layers and are given a permittivity of $80\epsilon_0$ (the same as water). The χ parameters are chosen with respect to the other segments as follows. The headgroup segments are given a preferential attraction to the surface by selecting $\chi_{PS} = -4$. In addition, the carbonlike segments are given a slight attraction for the surface, $\chi_{CS} = -2$. All other segments in solution are given a nonpreferential interaction with the surface by selecting the χ values to be zero. This particular surface will be hence referred to as the (420) surface. This notation illustrates the negative χ parameters with respect to the surface for the headgroup, aliphatic chain, and water.

(2) The second modeled surface has the same parameters except that the χ values with respect to the headgroup, aliphatic segments, and water are different. Our selection in this case is $\chi_{PS} = 0$, $\chi_{CS} = -3$, and $\chi_{WS} = -1$. Here we have taken away the preferential headgroup attraction to the surface, increased the aliphatic attraction slightly, and given water a bit of attraction for the surface. This second surface will be given the index (031).

Despite the differences in surface parameters, note that the displacement χ parameter with respect to the aliphatic segments is the same in both cases. We define the displacement χ parameter for some segment A as follows

$$\chi_{d,A} = \chi_{AS} + \chi_{WW} - \chi_{WS} - \chi_{AW} \quad (19)$$

This quantity represents the standard Gibbs energy of adsorption, i.e., the energy to exchange a water segment (W) on the surface with a segment A from bulk solution. With respect to the aliphatic segments (C), $\chi_{d,C} = -3.9$ for both the (420) and (031) surfaces. This means that both surfaces essentially have the same hydrophobicity. The main difference between the two surfaces studied here is the displacement χ for the headgroup. For the (420) surface, $\chi_{d,P} = -4$, whereas for the (031) surface, $\chi_{d,P} = +1$. This means that the headgroup has a preferential attraction for the (420) surface but a slight repulsion from the (031) surface.

We should also note that the calculations of adsorption are done with a flat lattice geometry. This means that we will be studying adsorption that occurs in flat structures even though this particular surfactant forms spherical micelles in bulk solution. Experiments often reveal different geometries between bulk and adsorbed aggregates (e.g., $C_{16}TAB$ forms spherical micelles in bulk solution but a flat layer on hydrophobized silica).³⁴ All our isotherms are truncated at the cmc because in experimental practice it is difficult to raise the surfactant chemical potential by further addition of surfactant above the cmc.

Results and Discussion

Surfactant in Bulk Solution. The aim of this paper is to examine surfactant adsorption on solid surfaces as a function of the separation between the two solids. As a prelude, we will

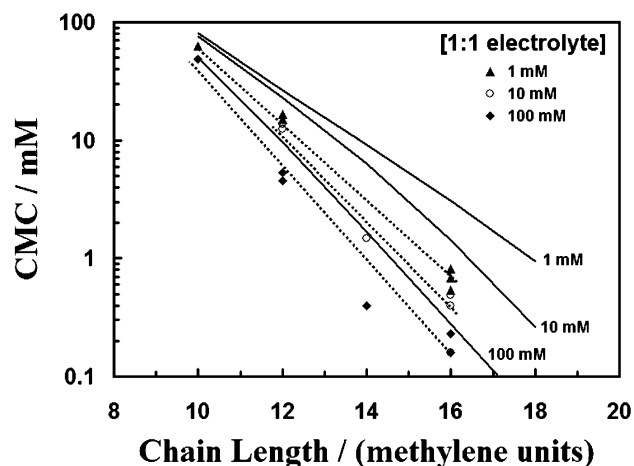


Figure 1. cmc vs surfactant chain length at various 1:1 electrolyte concentrations. The symbols represent experimental values taken from refs 11 and 39–41 for alkyl trimethylammonium and pyridinium surfactants. The dotted lines are merely guides for elucidation of the data sets. The solid lines represent the calculated values for $C_nP_3^+$ surfactants obtained with the SCFA Theory.

TABLE 2: cmc of $C_{16}P_3^+$ from SCFA at Various Monovalent Salt Concentrations

[salt]/mM	cmc/mM
1	3.08
5	2.05
10	1.43
20	0.895
50	0.456
100	0.279
200	0.176
500	0.104

give a brief discussion of the modeled bulk properties in order to show that the model parameters yield reasonable results compared to experimental literature. In addition, we will briefly discuss the structural and electrical properties of the modeled bulk aggregates. First we established that for our parameter choices, spherical micelles have a lower energy than cylindrical or bilayer micelles. This is consistent with experimental findings for ionic surfactants of similar chain length.^{35–38} Therefore, all cmc values presented are for calculations with spherical micelles. The cmc values calculated for $C_{16}P_3^+$ with our parameter selections are presented in Table 2.

As mentioned in the parameter section, our choice of χ_{CW} was chosen so that we obtain reasonable trends in the cmc with respect to surfactant chain length and ionic strength. Figure 1 shows several experimental values for the cmc of various alkyl trimethylammonium and pyridinium surfactants^{11,39–41} compared to the calculated values. Here our concern is that the slopes and trends with ionic strength are reasonable despite the fact that the quantitative agreement is not exact. The lack of quantitative agreement can result from several factors, including the modeling of the ω -methyl group, the headgroup, or the counterion. Studies have shown that the counterion can have a significant effect upon the cmc of ionic surfactants.⁴² Agreement of the change in the cmc with chain length means that the short-range hydrophobic effect is reasonably modeled by our parameter choices. This is critical for studies of adsorption and surfactant association.

Since the double-layer force is central to this paper, and such a force is dictated by the ionic strength in solution, we will focus our discussion of bulk properties on ionic strength effects.

In Figure 2 the distribution of segments in a micelle is given both for the tails and headgroups in the presence of 10 and 100

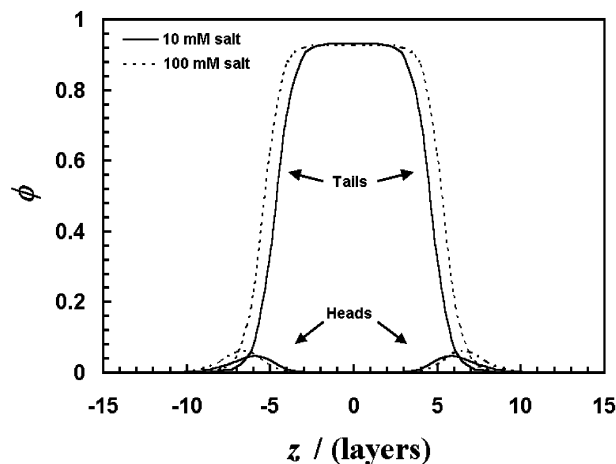


Figure 2. Radial segment distribution for $C_{16}P_3^+$ surfactants in a spherical micelle at salt concentrations of 10 and 100 mM. $z = 0$ is the center of mass of the micelle. Both the tail and headgroup distributions extend to higher layers as the ionic strength increases. $\chi_{AW} = 0$, $\chi_{CA'} = 2$, $\chi_{CW} = 1.9$.

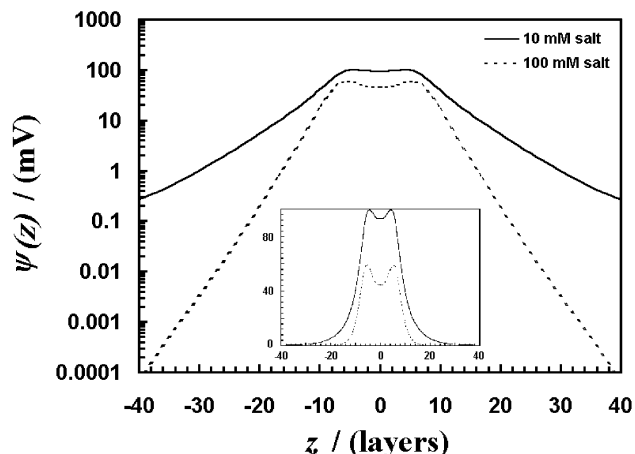


Figure 3. Electrical potential around a spherical micelle of $C_{16}P_3^+$ in 10 and 100 mM salt solutions. The y axis is on a log scale so the different decay lengths can easily be discerned. The inset shows the same data on a linear scale. The magnitude and range of the potential decreases with increased electrolyte concentration. The parameters are the same as in Figure 2.

mM monovalent salt. It is easy to see from Figure 2 that the tail groups occupy the center of the micelle (center of mass is $z = 0$). The headgroups are situated with a distribution over a couple of layers with a peak at about 6 or 7 lattice layers from the center of the micelle, depending upon ionic strength. This means that the micelles have diameters of about 3.7–4.3 nm. This micellar size, as well as the thicknesses of adsorbed layers discussed later, is underestimated by our current model due to the extra flexibility of the aliphatic tail imparted by the Markov approximation to calculate chain conformations as well as the fact that the excluded volume correlations are not treated rigorously.

An increase in the ionic strength causes the chain distribution to extend to higher layers. Therefore, there are more trans conformations, and the aggregation number is greater at higher ionic strengths. Furthermore, the additional screening of surfactant headgroups allows for a tighter packing of molecules in the micelle (notice narrower headgroup peak in Figure 2) and thus a higher aggregation number.

The electric potential profile around a $C_{16}P_3^+$ micelle is presented in Figure 3 for 10 and 100 mM monovalent salts.

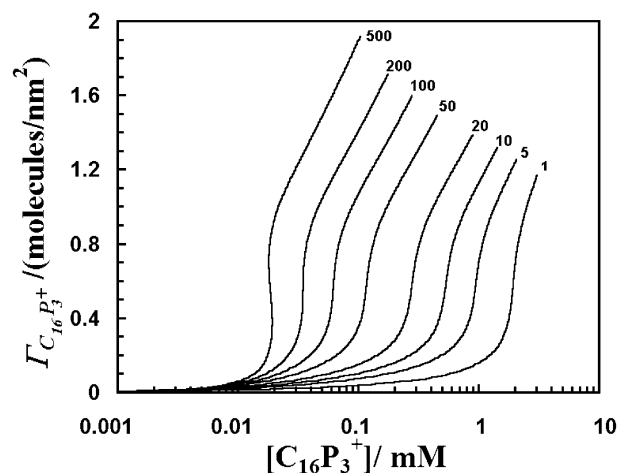


Figure 4. Adsorption as a function of $C_{16}P_3^+$ concentration at various electrolyte concentrations on an isolated, neutral surface (420). Each curve is labeled with the electrolyte concentration in units of mM. Adsorption increases as the salt concentration is raised. $\chi_{AW} = 0$, $\chi_{CA'} = 2$, $\chi_{CW} = 1.9$, $\chi_{CS} = -2$, and $\chi_{PS} = -4$.

The peaks in the potential correspond with the maximum volume fraction of headgroups. The calculated potential in solution decays exponentially at large z as the inverse square of the ionic strength (I) as is predicted by Poisson–Boltzmann theory

$$\kappa^{-1} = \frac{0.97 \text{ layers}}{(I/M)^{1/2}} = \frac{0.30 \text{ nm}}{(I/M)^{1/2}} \quad (20)$$

The coefficient of 0.30 nm is in agreement with the Poisson–Boltzmann theory for 1:1 electrolytes at 298 K.⁴³

Within the micelle, the decay length is much longer because the permittivity and electrolyte concentration within the micelle is much lower. Furthermore, the potential (at the maximum headgroup density) is lower at higher ionic strengths. This decrease in micelle electrical potential is non-Nernstian with salt concentration. In this case, the slope is only −40 mV per decade. This is because the potential determining ions are not the salt ions but rather the surfactant ions, whose characteristic concentration is the cmc. The ionic strength affects the potential by changing the value of the cmc. The micelle potential scales with the ionic strength dependent cmc, $\text{cmc}(I)$, in a Nernstian fashion. Here we find that

$$\frac{\partial \psi_{\text{micelle}}}{\partial \log[\text{cmc}(I)]} = 58 \text{ mV} \quad (21)$$

Adsorption at Large Separations. SCFA isotherms and segment profiles for isolated surfaces are not new to the literature;^{12,20–22,44} however, they provide an appropriate initial discussion for this study. We will begin our discussion of adsorption by presenting the calculated adsorption isotherms as a function of ionic strength in solution for the (420) surface. In the isotherms presented in Figure 4, we see the basic features associated with adsorption on a solid, uncharged surface. Adsorption initially rises slowly. The hydrophobic tails are attracted to the surface, but there is a repulsive interaction between the charged headgroups of neighboring surfactants on the surface. This is clearly shown at lower salt concentrations by the smaller slope in the adsorption isotherm due to longer range headgroup repulsions. Once the tails reach a given density on the surface, the adsorption begins to rise steeply due to a loss of unfavorable C–W interactions. As the surfactant

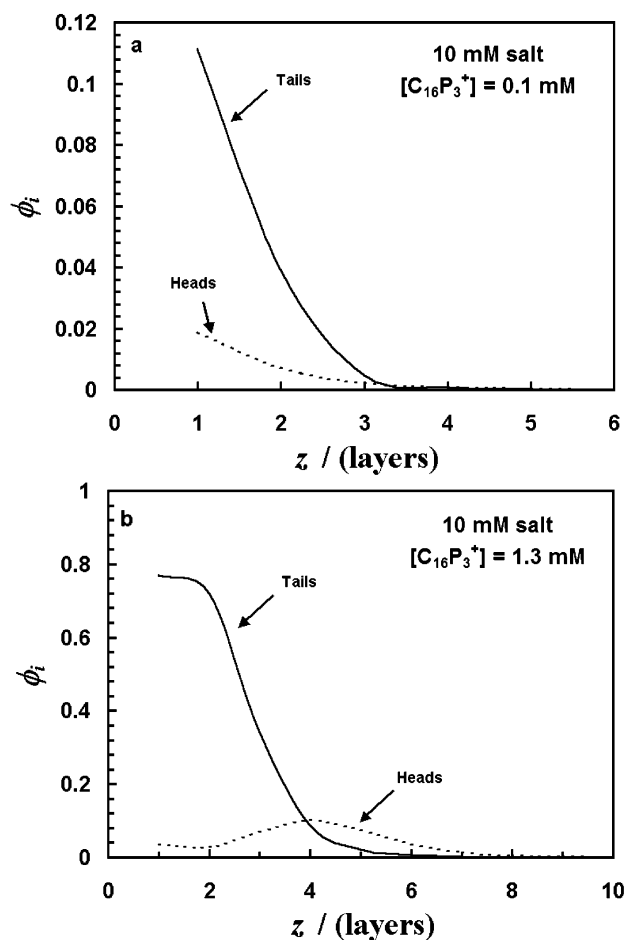


Figure 5. Segment distributions for two $C_{16}P_3^+$ concentrations near an isolated, neutral (420) surface. (a) At low concentrations, the surfactant lies almost flat on the surface with both the headgroups and tails in the first 2 layers. Note: there are 16 tails groups for every 3 headgroups. (b) At higher concentrations, the ratio of tails to heads is greater in the first layer. The surfaces are separated by $H = 70$ lattice layers. The parameters are the same as in Figure 4.

concentration approaches the cmc, the electrostatic repulsion between headgroups causes a decrease in the slope of the isotherm.

In addition, the isotherms in Figure 4 show the expected increase in the adsorption plateau at higher ionic strengths due to the increased screening of headgroup repulsions. This screening also shifts the step in the isotherm to lower surfactant concentrations because there is a smaller repulsive force between the headgroups.

The average orientation of the surfactant with respect to the surface can be deduced from the density profile. Figure 5 shows examples in 10 mM electrolyte solution. At low surfactant concentrations, the headgroup is attracted to the surface along with the tails and the surfactant adsorbs relatively flat on the surface. At high concentrations, closer to the cmc (Figure 5b), the number of tail–tail interactions is larger and the surfactant is primarily oriented with its charged head toward the solution.

Adsorption at Decreased Separations. Our goal here is to present the effects of the interaction between two identical surfaces on the adsorption isotherms. We reduce the separation between the modeled surfaces by reducing the number of lattice layers between the two solids. Figure 6 shows a series of adsorption isotherms calculated at different solid–solid separations for the (420) surface at a constant monovalent salt concentration of 10 mM.

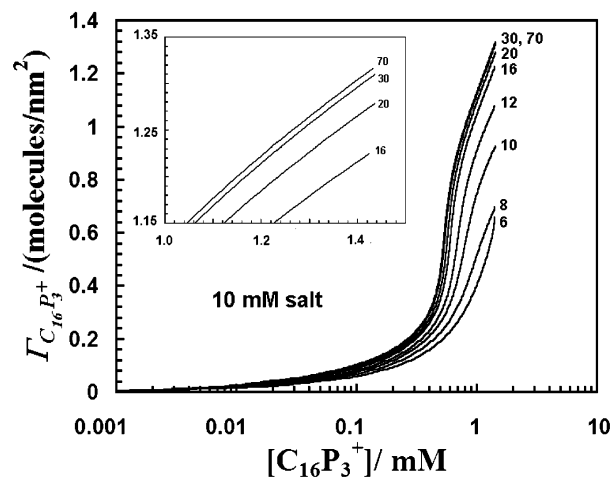


Figure 6. Adsorption as a function of $C_{16}P_3^+$ concentration at various solid–solid separations on a neutral (420) surface in 10 mM salt. The separation is listed next to the respective curve in units of lattice layers. The amount adsorbed decreases as the separation is made sufficiently small. The inset shows the data for separations 16, 20, 30, and 70. The adsorption is essentially constant (to within 1%) until the separation falls below about 30 layers $\sim (3\kappa^{-1})$. The parameters are the same as for Figure 4.

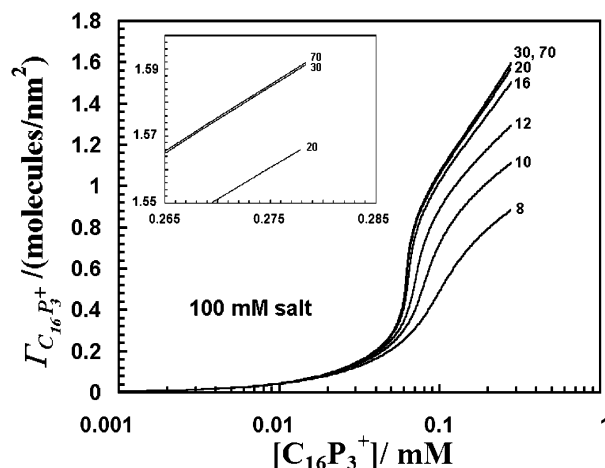


Figure 7. Adsorption as a function of $C_{16}P_3^+$ concentration at various solid–solid separations on a neutral (420) surface in 100 mM salt. The separation is listed next to the respective curve in units of lattice layers. A smaller separation is required to cause desorption in 100 mM vs 10 mM salt. The parameters are the same as in Figure 4.

Figure 6 shows that the adsorption has the same general shape at smaller separations, however, the magnitude in the adsorption changes considerably. Changes in adsorption become significant when the separation between the solids is less than about $3\kappa^{-1}$ when the electric double-layers begin to overlap. The largest absolute changes in adsorption with separation occur at surfactant concentrations at or above the step in the isotherm. For example, at 0.6 mM $C_{16}P_3^+$, the absolute adsorption changes from 0.77 molecules/nm² at $H = \infty$ to 0.39 molecules/nm² at $H = 12$ layers. A drastic change in adsorption occurs when the step in the isotherm is very steep.

An increase in the electrolyte concentration yields isotherms with the same general shape (Figure 7); however, since at larger separations the regulating force is the double-layer force, we should expect that the deviation is smaller if the double-layer force is shorter-ranged. At the cmc in 10 mM salt (1.43 mM), the change in adsorbed amount was 1% going from a separation

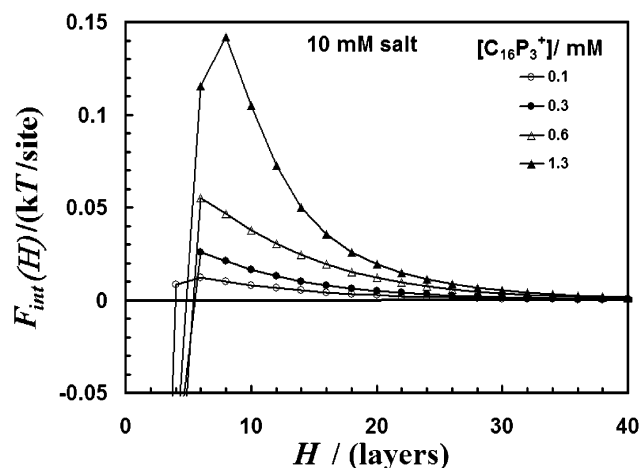


Figure 8. The interaction energy is plotted as a function of separation for neutral (420) surfaces in 10 mM salt. As the concentration of surfactant increases, the interaction energy also increases. The parameters are the same as in Figure 4.

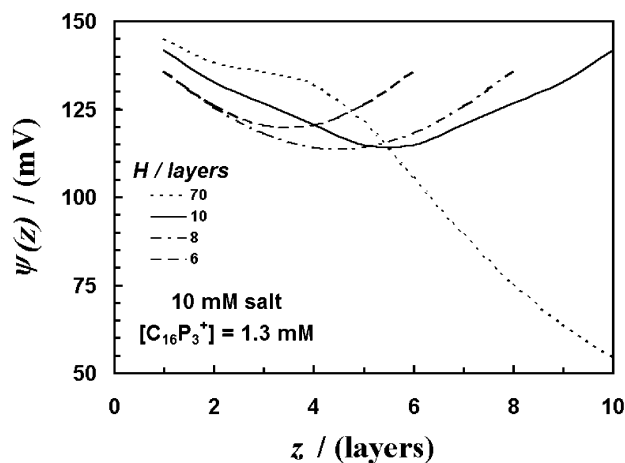


Figure 9. The electrical potential as a function of distance from the solid for various separations between the two solids (70, 10, 8, and 6 layers). $[C_{16}P_3^+] = 1.3$ mM and [salt] = 10 mM. The parameters are the same as in Figure 4.

of 70 to 30 layers; however, at the cmc in 100 mM salt (0.279 mM), the change is now less than 0.1% over the same separations.

We are also interested in calculating the interactions between solid surfaces with adsorbed surfactant layers present. Figure 8 shows the interaction energy as a function of solid–solid separation, H . The interaction energy is repulsive (positive) for $H > 6$ –8 layers. Furthermore, at larger separations, the interaction becomes more repulsive as the surfactant concentration increases. This results from a greater electric potential due to the presence of a higher density of charged surfactant on the surfaces.

In Figure 9, the electric potential profiles are shown for $[C_{16}P_3^+] = 1.3$ mM. This concentration is 0.9 cmc but still results in a large absolute adsorption. In general, the potential at the midplane between the solids, $\psi((H/2))$, increases as the surfaces approach. There is a slight change in behavior for $6 < H < 10$ layers. The midplane potential is actually a bit lower at a separation of $H = 8$ than $H = 10$ layers. The values for the midplane potentials are given in Table 3. Such a local maximum in the electric potential results from a change in the shape of the potential profile as the adsorbed layers on both surfaces begin to merge. This corresponds to the maximum in the

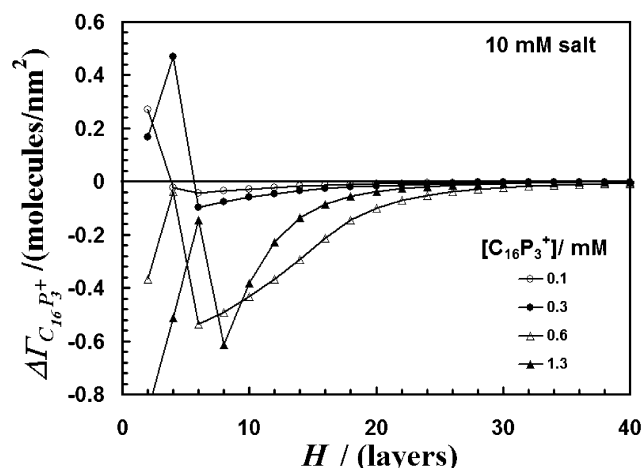


Figure 10. The change in surface excess for $C_{16}P_3^+$ is plotted vs separation for neutral (420) surfaces in 10 mM salt. The surfactant desorbs as the surfaces interact. The parameters are the same as in Figure 4.

TABLE 3: Electric Potentials at the Midplane between Two Flat, Uncharged (420) Surfaces ($[C_{16}P_3^+] = 1.3$ mM)

H/layers	$\psi((H/2))/\text{mV}$
70	3.84
30	41.3
20	70.7
16	88.5
12	108
10	115
8	114
6	120

interaction energy presented in Figure 8 and will be discussed in more detail later.

In Figure 10 we plot the change in adsorption as a function of solid–solid separation for the same four surfactant concentrations as in Figure 8. Such a plot allows us to easily see the quantitative differences in the adsorption as a function of separation between the two solids. We will now discuss the mechanisms that lead to the adsorption changes in Figure 10.

For $H > 10$ layers, the change in adsorption shows a maximum with respect to concentration around 0.6 mM. The magnitude of the adsorption regulation increases up to 0.6 mM and decreases thereafter. This is because at 0.6 mM the surfactant concentration is near a pseudo phase transition (the step in the isotherm, Figure 6). At such a concentration, small deviations in confinement can lead to large changes in the adsorption behavior, just as small changes in concentration cause large changes in adsorption for an isolated surface

At smaller separations, the step in the isotherm occurs at higher concentrations (Figure 6). According to our previous hypothesis, the desorption should be a maximum at higher concentrations. Indeed this is the case at $8 < H < 10$ layers, as is shown in Figure 10. At the step in the isotherm, the electrostatic potential increases sharply due to surfactant adsorption, and it is the regulation of this potential that drives the adsorption changes upon confinement.

At small separations ($H < 8$ layers), we see very interesting behavior in Figure 10. The surfactant desorbs, adsorbs, and then desorbs again. To further understand this behavior, we have plotted the segment density profiles for the tail and headgroup segments at $[C_{16}P_3^+] = 1.3$ mM (Figure 11). At this particular concentration, the maximum in the interaction energy occurs at $H = 8$ layers (Figure 8).

At $6 < H < 8$ layers in Figure 11a, we notice that the tail density is nonzero everywhere between the surfaces. This means

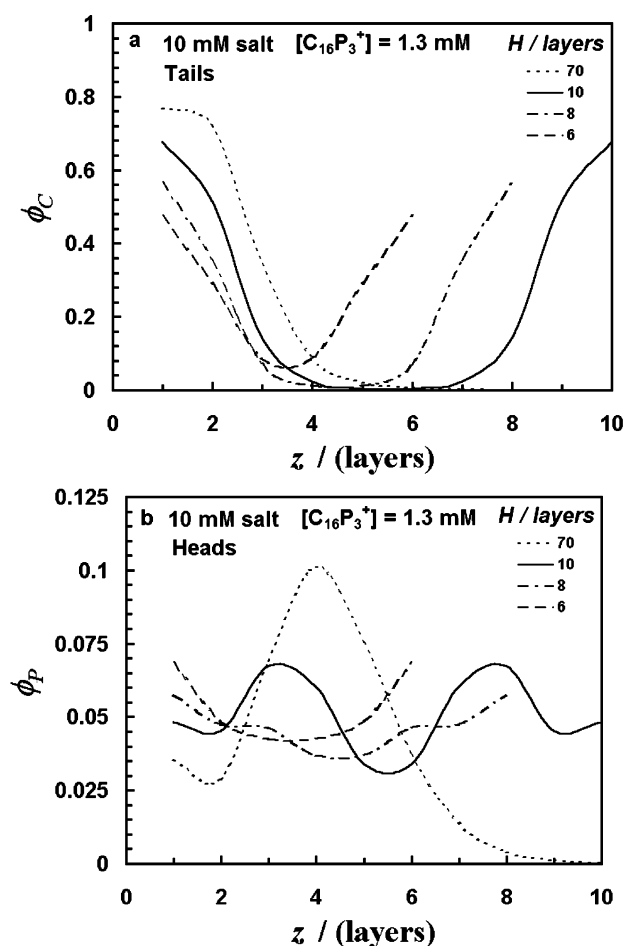


Figure 11. Density profiles of tail segments (C) and headgroup segments (P) in the vicinity of a (420) surface is shown as a function solid–solid separation. The separation is listed in the figure in units of lattice layers. All curves shown are for $[C_{16}P_3^+] = 1.3$ mM in the presence of 10 mM salt. The parameters are the same as in Figure 4.

that the surfactant tails on one solid are interacting with the tails from the second solid. Such a favorable carbon–carbon vs carbon–water interaction promotes adsorption, and we see the value of $\Delta\Gamma_{C_{16}P_3^+}$ becomes more positive. At lower concentrations, this is seen at smaller separations because the chains do not extend as far from the surface (Figure 5). A large change in adsorption at very small separations has been postulated experimentally as being the result of the increased hydrophobic effect between interacting adsorbed layers.^{5,6,11,45}

As the separation is decreased further, the headgroup density continues to merge (Figure 11b). At $H = 6$ layers, the headgroup density becomes parabolic between the surfaces and subsequent decreases in separation increase the electrical potential everywhere between the surfaces. In addition, the number of possible conformations for the surfactant in the film between the solids is decreased. The entropic cost of losing conformations can lead to a depletion of surfactant from the solid surface.

Such a complicated interaction between the adsorbed layers on each solid at very small separations contributes to the local extrema in the electric potential at $H = 8$ and 10 layers as mentioned earlier. It seems as though such a drastic change in adsorption behavior at these separations (Figure 10) is too large to be attributed to such a small midplane potential difference (Table 3). This shows the importance of the overlap of hydrophobic tails between two interacting adsorbed surfactant layers.

Furthermore, Figure 11b shows an interesting feature that has relevance to the analysis of experimental interparticle force measurements. Notice that the peak in the headgroup density moves closer to the solid surfaces as a second solid approaches. This means that the surfactant layer is being compressed as the interaction energy rises in Figure 8. If we define the thickness of the adsorbed surfactant layer, t , as the number weighted average location of headgroup segments, then we can calculate the fractional thickness, $\Theta(H)$, of the surfactant layer as the separation is decreased to H

$$\Theta(H) = \frac{t(H)}{t(\infty)} \quad (22)$$

Figure 11 shows the fractional thickness as a function of solid–solid separation. At the separation where the maximum interaction energy occurs ($H = 8$ layers), the surfactant layer has been compressed to about 60% of its original thickness. This has particular importance when trying to fit DLVO theory to experimental interaction energies in surfactant solutions. For simplicity, it is customary to fit the double-layer potential by assuming that there is a plane of charge at a fixed distance from the solid surface (i.e., constant adsorbed film thickness). In contrast, our calculations show that the adsorbed film thickness diminishes significantly during the interaction. The planes of charge therefore, approach each other to a smaller degree than the solid surfaces approach each other. This is regulation of film thickness as well as charge density (by the desorption of surfactant). At even smaller solid–solid separations, the segment densities (Figure 11) show hydrocarbon density at all separations. The film profiles are highly distorted from those at $H = 70$ layers and it is not clear that adsorption should be treated as still occurring in two discrete layers; the adsorbed layers have merged. An increase in ionic strength suppresses the film thinning until smaller separations, implying that electrostatic forces between the films on opposite surfaces promote film thinning. We must remember when interpreting these results that the chain flexibility is overestimated in these calculations.

We will now relate our findings to the experimental practice of measuring surfactant layer thickness using atomic force microscopy (AFM) or the surface forces apparatus (SFA). It is common practice to use the separation at the onset of mechanical instability as an indication of the film thickness.^{46–51} The relationship between these parameters is complex. The mechanical instability occurs when the force gradient equals the spring constant of the AFM or SFA cantilever. This can occur for any attractive force (e.g., van der Waals) and does not require a surfactant layer. Here we explore a different issue, the extent of compression of the film thickness by an opposing solid surface at the maximum force. (Note the differences in geometry between AFM measurements and our calculations.) If we assume that the mechanical instability occurs in the vicinity of the maximum interaction energy ($H = 8$ layers or 2.5 nm) in 1.3 mM $C_{16}P_3^+$, then equating this separation to twice the adsorbed film thickness yields a surfactant film 4 lattice layers (1.25 nm) thick per surface. At this solid–solid separation, the film has been distorted and there is a high headgroup density at all z . The film layer thickness of 4 lattice layers predicted from interaction energy maximum does, perhaps by coincidence, correspond to the maximum in headgroup density at $H = \infty$. This agreement appears to be the result of the partial cancellation of two effects. The film has been thinned; however, the instability occurs when there is a gap between the maxima in headgroup density.

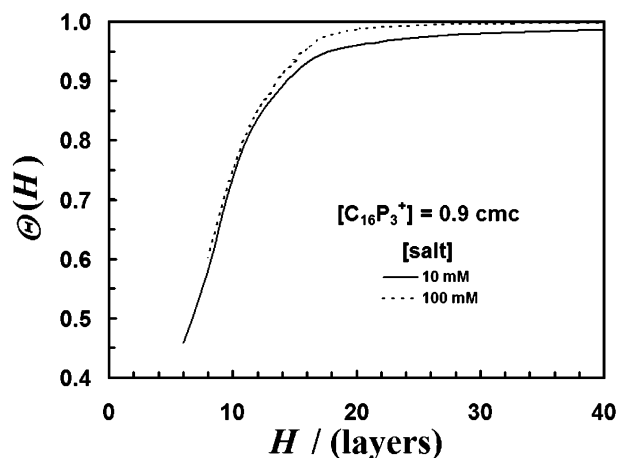


Figure 12. Fractional thickness of the surfactant layer as a function of solid–solid separation for the (420) surface at 0.9 cmc $C_{16}P_3^+$ (1.3 mM at [salt] = 10 mM and 0.25 mM at [salt] = 100 mM). The layer is compressed as the surfaces approach. The parameters are the same as in Figure 4.

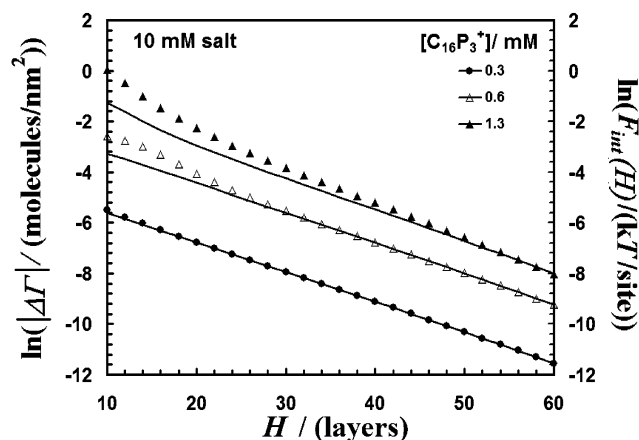


Figure 13. The natural logarithm of $\Delta\Gamma$ (symbols) and the interaction energy (solid lines) are plotted vs separation. The intercept has been shifted for each $\Delta\Gamma$ in order to better see the changes in slope. The parameters are the same as in Figure 4.

Comparison of Adsorption and Energy Decay Lengths.

Figure 13 shows the natural logarithm of both the interaction energy and the changes in surface excess as a function of solid–solid separation. At surfactant concentrations up to the step in the adsorption isotherm, the adsorption decay length is equal to the Debye length. Therefore, proximal adsorption of surfactant is dominated by electrostatic forces. We should note that the interaction-free energy decays with a slightly smaller decay length than that predicted by Poisson–Boltzmann theory.

At 0.6 mM and 1.3 mM $C_{16}P_3^+$, there is a slight deviation in decay lengths between the interaction energy and the adsorption. The slope of the adsorption is greater than the slope of the force. In this separation regime, there is a strong overlap of the double layers, and the double-layer interaction can no longer be represented by a simple exponential.

Electrolyte Adsorption/Desorption Behavior. All ions in solution contribute to the regulation of the solid–solid interaction. Here we will track the behavior of the inert salt ions in solution during the solid–solid interaction in order to deduce their contributions.

In Figure 14a, we see that desorption of B^- mirrors that of the surfactant, however to a smaller extent. This is because, at infinite separation, the surface charge (charge from adsorbed

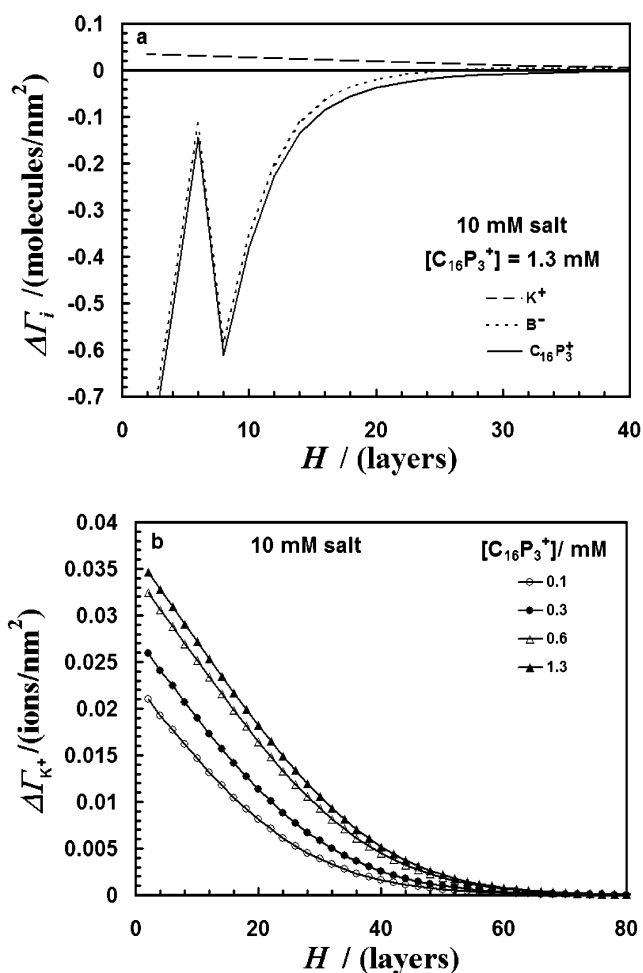


Figure 14. (a) Change in surface excess for K^+ , B^- , and $C_{16}P_3^+$ vs solid–solid (420) separation in 10 mM salt at $[C_{16}P_3^+] = 1.3$ mM. (b) Change in surface excess for K^+ vs solid–solid separation in 10 mM salt at different surfactant concentrations. K^+ adsorbs as the surfaces interact. The parameters are the same as in Figure 4.

surfactant) is largely compensated by adsorption of counterions and to a smaller extent by exclusion of co-ions.

As the separation between the solids is decreased, the surfactant desorbs and the co-ion exclusion (desorption) is less. This is seen as an adsorption of K^+ compared to infinite separation (Figure 14). This gives a good indication of how the surfactant desorbs *without* its counterion, since the value of $\Delta\Gamma$ for the surfactant desorbing *without* a counterion is simply the negative of the change in adsorption for K^+ .

Furthermore, as the solid–solid separation decreases and the surfactant desorbs, the loss of co-ion exclusion plays a much larger role in the charge compensation because the surface potential is becoming less positive. This is expected from the Poisson–Boltzmann theory, where the ratio $(\Gamma_{K^+}/\Gamma_{B^-})$ will go from zero at $\psi(0) = +\infty$ to unity at $\psi(0) = 0$.

If we compare the magnitudes of the surfactant desorption with and without a counterion, we see an interesting phenomenon. As the surfactant desorbs, the potential becomes less positive close to the surface where the surfactant is adsorbed (see Figure 9). Therefore, the negative counterion is less favored near the surface. As a consequence, the counterion can leave more readily with the surfactant. Even though the number of surfactants that desorb *without* their counterion is increasing with decreased separation, the fraction of those desorbing *without* a counterion actually decreases due to the increased desorption of B^- .

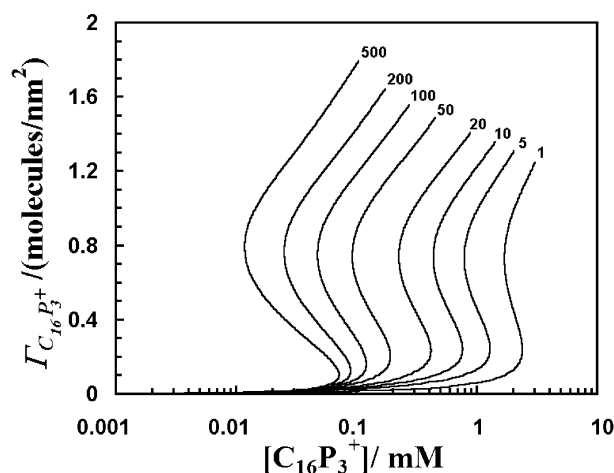


Figure 15. Adsorption isotherms for $C_{16}P_3^+$ on an isolated, neutral surface (031) as a function of electrolyte concentration. Each curve is labeled with the electrolyte concentration in units of mM. Adsorption increases as the salt concentration is raised. $\chi_{AW} = 0$, $\chi_{CA'} = 2$, $\chi_{CW} = 1.9$, $\chi_{CS} = -3$, and $\chi_{WS} = -1$.

Adsorption When the Headgroup Has a Low Affinity for the Surface. Here we will discuss the effects of solid–solid interactions for a set of parameters that yield isotherms with a discontinuous step (s-shaped loop). For the solid labeled (031), the headgroup is not attracted to the solid ($\chi_{PS} = 0$), but water does have an affinity for the solid surface ($\chi_{WS} = -1$). Therefore, the key difference between the (031) and (420) surfaces is that the displacement χ parameter for the headgroup is $\chi_{dP} = +1$ for the (031) surface. The displacement χ parameter for the alkyl tails is the same as for the (420) surface.

Such loops in the isotherm have been discussed previously in SCFA calculations.^{20,22,30} Along this loop there are multiple values of the surface excess for a single surfactant concentration. At the step in the isotherm there are two stable surface excess values and one unstable value for the same surfactant concentration. At other concentrations along the loop there are metastable values of the surface excess.

In Figure 15, it is easy to see that the size of the loop increases with increased salt concentration. This was also the case for the (420) surface, with a small loop appearing at 500 mM salt. Furthermore, the adsorption for (031) is suppressed until higher surfactant concentrations compared to the (420) surface. The surfactant chemical potential in the bulk must be much higher to force the surfactant to adsorb and displace the water.

For (031) isotherms, the confinement by another surface also decreases the plateau adsorption and shifts the adsorption curve to higher concentrations. Above and below the step in the isotherm, the trends are the same as for the (420) surface. Below the step, however, both the interaction energy and change in adsorption are less in magnitude at a given concentration for (031) than for (420). This results from the fact that the surface excess is lower in this region due to the increased affinity of water for the surface. The lower amount of adsorbed surfactant leads to a lower positive potential between the surfaces and thus a decreased interaction energy. This leads to a decreased driving force for proximal desorption for most concentrations compared to the (420) surface.

Once again, there is interesting behavior near the step in the isotherm. Because of the discontinuous nature of the step, however, an analysis near the step such as that shown for the (420) surface is much more complicated. As the separation is decreased, the step in the isotherm shifts to higher surfactant concentrations as shown in Figure 16. As a consequence, the

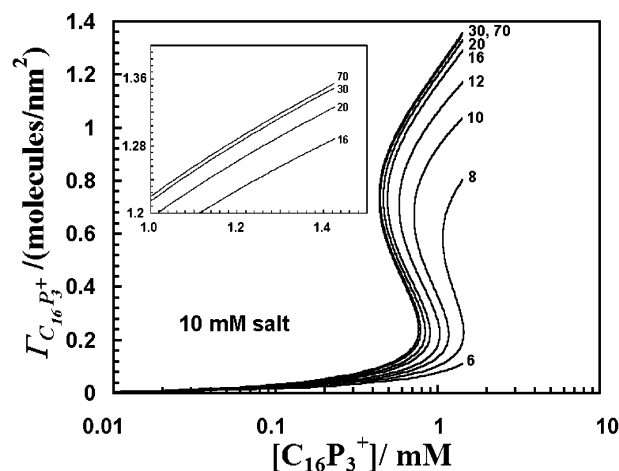


Figure 16. Adsorption isotherms as a function of solid–solid separation on a neutral (031) surface in 10 mM salt. The separation is listed next to the respective curve in units of lattice layers. The amount adsorbed decreases as the separation is made sufficiently small. The inset shows the data for separations 16, 20, 30, and 70. At 30 layers, the adsorption is a bit lower than for 70 layers. The parameters are the same as in Figure 15.

adsorption can either traverse a metastable branch of the isotherm (along the loop) or jump to a much lower equilibrium value. If the adsorption follows the metastable regimes upon compression and separation of the surfaces, a hysteresis develops in the adsorption vs separation as well as the interaction energy vs separation. Otherwise, the adsorption can jump between two different, but stable, surface excess values. This can lead to large proximal desorption at concentrations in the vicinity of the discontinuous step in the isotherm. The metastable behavior is complicated and therefore will be discussed in a subsequent publication (Koopal, L. K.; Leermakers, F. A. M.; Lokar, W. J.; Ducker, W. A. *J. Phys. Chem. B* Submitted).

In Figure 17, we present the interaction curves and the changes in the adsorbed amount brought about by confinement of the surfaces. Once again at the concentrations shown, the behavior is very similar to that shown for the (420) surface; however, the magnitude of surfactant that desorbs at $H < 8$ layers in 1.3 mM surfactant is greatly increased due to structural differences in the adsorbed layer brought about by the differences in head, tail, and water interaction with the (031) surface.

Conclusions

The adsorption of a model ionic surfactant on a neutral, slightly hydrophobic flat surface has been studied as a function of the interaction with a second identical surface. A strong repulsive force is created by the presence of an adsorbed charged surfactant layer.

During the approach of the second solid, the adsorbed layer of surfactant responds so as to reduce the repulsive force that would otherwise occur. This response consists of desorption of surfactant and counterions, adsorption of co-ions, and a thinner layer of surfactant. Ultimately, the surfactant layers on the two solids begin to merge. The largest desorption of surfactant occurs at or above the surfactant concentration where there is a steep rise in the adsorption–concentration curve. Closer approach of the solids shifts the position of this steep rise to higher surfactant concentrations. The shift in this curve makes the adsorption very sensitive to the separation between the solids.

When the headgroups do not have an affinity for the solid ((031) surface), the adsorption shows an s-shaped isotherm and

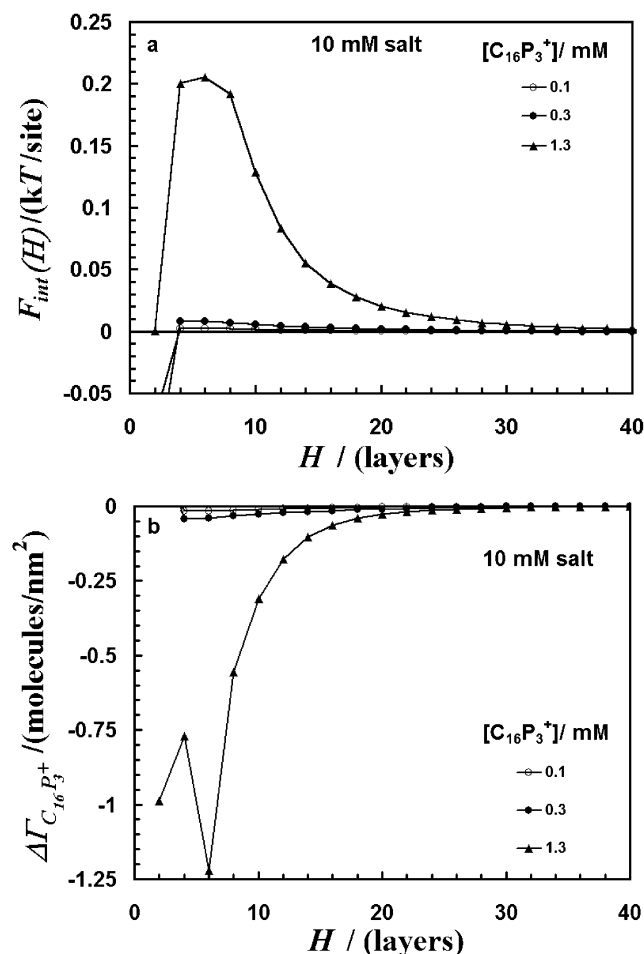


Figure 17. (a) Interaction energy as a function of separation for neutral (031) surfaces in 10 mM salt. As the concentration of surfactant increases, the interaction energy also increases. (b) The change in surface excess for $C_{16}P_3^+$ is plotted vs separation for neutral (031) surfaces in 10 mM salt. The surfactant desorbs as the surfaces interact. The parameters are the same as in Figure 15.

is even more responsive to the approach of another solid near the step in the isotherm. A small change in separation can cause switching between branches of the adsorption curve and bring about large changes in adsorption.

Acknowledgment. This work is based on research supported by the National Science Foundation Grant CHE-0203987. W. J. Lokar thanks Wageningen University in The Netherlands for hosting him for the duration of this project.

References and Notes

- (1) Ninham, B. W.; Parsegian, V. A. *J. Theor. Biol.* **1971**, *31*, 405–428.
- (2) Hall, D. G. *J. Chem. Soc., Faraday Trans. 2* **1972**, *68*, 2169–2182.
- (3) Ash, S. G.; Everett, D. H.; Radke, C. J. *J. Chem. Soc., Faraday Trans. 2* **1973**, *69*, 1256–1277.
- (4) Pethica, B. A. *Colloids Surf., A* **1995**, *105*, 257–264.
- (5) Rutland, M. W.; Parker, J. L. *Langmuir* **1994**, *10*, 1110–1121.
- (6) Yaminsky, V. V. *Langmuir* **1994**, *10*, 2710–2717.
- (7) Podgornik, R.; Parsegian, V. A. *J. Phys. Chem.* **1995**, *99*, 9491–9496.
- (8) Christenson, H. K.; Yaminsky, V. V. *Colloids Surf., A* **1997**, *129–130*, 67–74.
- (9) Lokar, W. J.; Ducker, W. A. *Langmuir* **2002**, *18*, 3167–3175.
- (10) Subramanian, V.; Ducker, W. J. *J. Phys. Chem. B* **2001**, *105*, 1389–1402.
- (11) Lokar, W. J.; Ducker, W. A. *Langmuir* **2004**, *20*, 378.
- (12) Scheutjens, J. M. H. M.; Fleer, G. J. *J. Phys. Chem.* **1979**, *83*, 1619–1635.
- (13) Scheutjens, J. M. H. M.; Fleer, G. J. *J. Phys. Chem.* **1980**, *84*, 178.
- (14) Meijer, L. A.; Leermakers, F. A. M.; Lyklema, J. *J. Chem. Phys.* **1999**, *110*, 6560–6579.
- (15) Oversteegen, S. M. *Phys. Rev. E: Stat. Phys., Plasmas, Fluids, Relat. Interdiscip. Top.* **2000**, *62*, 8453–8461.
- (16) Leermakers, F. A. M.; Scheutjens, J. M. H. M.; Lyklema, J. *Biophys. Chem.* **1983**, *18*, 353–360.
- (17) Böhmer, M. R.; Koopal, L. K. *Langmuir* **1992**, *8*, 2660–2665.
- (18) Böhmer, M. R.; Koopal, L. K.; Lyklema, J. *J. Phys. Chem.* **1991**, *95*, 9569–9578.
- (19) Koopal, L. K.; Lee, E. M.; Böhmer, M. R. *J. Colloid Interface Sci.* **1995**, *170*, 85–97.
- (20) Goloub, T. P.; Koopal, L. K. *Langmuir* **1997**, *13*, 673–681.
- (21) Böhmer, M. R.; Koopal, L. K. *Langmuir* **1992**, *8*, 2649–2659.
- (22) Jódar-Reyes, A. B.; Ortega-Vinuesa, J. L.; Martín-Rodríguez, A.; Leermakers, F. A. M. *Langmuir* **2003**, *19*, 878–887.
- (23) Vermeer, A. W. P.; Leermakers, F. A. M.; Koopal, L. K. *Langmuir* **1997**, *13*, 4413–4421.
- (24) Wolterink, J. K.; Leermakers, F. A. M.; Fleer, G. J.; Koopal, L. K.; Zhulina, E. B.; Borisov, O. V. *Macromolecules* **1999**, *32*, 2365–2377.
- (25) Wijmans, C. M.; Scheutjens, J. M. H. M.; Zhulina, E. B. *Macromolecules* **1992**, *25*, 2657–2665.
- (26) Israëls, R.; Leermakers, F. A. M.; Fleer, G. J. *Macromolecules* **1994**, *27*, 3087–3093.
- (27) Sader, J. E.; Chan, D. Y. C. *Langmuir* **2000**, *16*, 324–331.
- (28) Wijmans, C. M.; Leermakers, F. A. M.; Fleer, G. J. *J. Colloid Interface Sci.* **1994**, *167*, 124–134.
- (29) Böhmer, M. R.; Koopal, L. K.; Tijssen, R. *J. Phys. Chem.* **1991**, *95*, 6285–6297.
- (30) Böhmer, M. R. *Adsorption and Micellization of Surfactants*, Ph.D. Thesis, Wageningen Agricultural University, 1991.
- (31) Flory, P. *Principles of Polymer Chemistry*; Cornell University Press: Ithaca, New York, 1953.
- (32) Van Lent, B.; Scheutjens, J. M. H. M. *Macromolecules* **1989**, *22*, 1931.
- (33) Tanford, C. *The Hydrophobic Effect*; Wiley-Interscience: New York, 1980.
- (34) Grant, L. M.; Tiberg, F.; Ducker, W. A. *J. Phys. Chem. B* **1998**, *102*, 4288–4294.
- (35) Pisarcik, M.; Devinsky, F.; Svajdlenka, E. *Colloids Surf., A* **1996**, *119*, 115–122.
- (36) Ozeki, S.; Ikeda, S. *Bull. Chem. Soc. Jpn.* **1981**, *54*, 552–555.
- (37) Imae, T.; Kamiya, R.; Ikeda, S. *J. Colloid Interface Sci.* **1985**, *108*, 215–225.
- (38) Fujio, K. *Bull. Chem. Soc. Jpn.* **1998**, *71*, 83–89.
- (39) van Os, N. M.; Haak, J. R.; Rupert, L. A. M. *Physico-Chemical Properties of Selected Anionic, Cationic, and Nonionic Surfactants*; Elsevier: Amsterdam, 1993.
- (40) Mehrian, T.; de Keizer, A.; Korteweg, A. J.; Lyklema, J. *Colloids Surf.* **1993**, *71*, 255–267.
- (41) Goloub, T. P.; Koopal, L. K.; Bijsterbosch, B. H.; Sidorova, M. P. *Langmuir* **1996**, *12*, 3188–3194.
- (42) Berr, S.; Jones, R. R. M.; Johnsson, J. S., Jr. *J. Phys. Chem.* **1992**, *96*, 5611–5614.
- (43) Israelachvili, J. N. *Intermolecular and surface forces*, 2nd ed.; Academic Press London: London, 1991.
- (44) Böhmer, M. R.; Koopal, L. K.; Janssen, R.; Lee, E. M.; Thomas, R. K.; Rennie, A. R. *Langmuir* **1992**, *8*, 2228–2239.
- (45) Claesson, P. M.; Kjellin, U. R. M. In *Surfactant Science Series*; Binks, B. P., Ed.; Marcel Dekker Inc.: New York, 1999; Vol. 83, pp 255–333.
- (46) Pashley, R. M.; Israelachvili, J. N. *Colloids Surf.* **1981**, *2*, 169.
- (47) Wanless, E. J.; Ducker, W. A. *J. Phys. Chem.* **1996**, *100*, 3207–3214.
- (48) Kékicheff, P.; Christenson, H. K.; Ninham, B. W. *Colloids Surf.* **1989**, *40*, 31–41.
- (49) Patrick, H. N.; Warr, G. G.; Manne, S.; Aksay, I. A. *Langmuir* **1999**, *15*, 1685–1692.
- (50) Wanless, E. J.; Ducker, W. A. *Langmuir* **1997**, *13*, 1463–1474.
- (51) Liu, J.-F.; Ducker, W. A. *J. Phys. Chem. B* **1999**, *103*, 8558–8567.